[1]O. Hachenberg and W. Brauer, in *Advances in Electronics and Electron Physics XI*, edited by L. Marton (Academic, New York, 1959).
[2]A. J. Dekker, in *Solid State Physics*, edited by F. Seitz and D. Turnbull (Academic, New York, 1959), Vol. 6.
[3]P. R. Thornton, *Scanning Electron Microscopy* (Chapman and Hall, London, 1968).
[4]J. L. H. Jonker, Philips Res. Rept. 6, 372 (1951); 12, 249 (1957).
[5]H. Stoltz, Ann. Physik 3, 197 (1959).
[6]J. Burns, Phys. Rev. 119, 102 (1960).
[7]See, for example, A. I. Titov, Fiz. Tverd. Tela 10, 1891 (1968) [Sov. Phys. Solid State 10, 1489 (1968)]; A. R. Shulman, V. V. Korablev, and Yu. A. Morozov, *ibid.* 10, 1913 (1968) [*ibid.* 10, 1512 (1968)]; A. B. Laponsky and N. R. Whetten, Phys. Rev. 120, 801 (1960).
[8]See, for example, A. J. Dekker, Phys. Rev. Letters 4, 55 (1960); R. M. Stern and H. Taub, *ibid.* 20, 1340 (1968); H. Taub, R. M. Stern, and V. F. Dvoryankin, Phys. Status Solidi 33, 573 (1969).
[9]H. A. Bethe, M. E. Rose, and L. P. Smith, Proc. Am. Phil. Soc. 78, 573 (1938).
[10]H. S. Snyder and W. T. Scott, Phys. Rev. 76, 220 (1949).
[11]H. W. Lewis, Phys. Rev. 78, 526 (1950).
[12]L. V. Spencer, Phys. Rev. 98, 1597 (1955).
[13]G. D. Archard, J. Appl. Phys. 32, 1505 (1961).
[14]T. E. Everhart, J. Appl. Phys. 31, 1483 (1960).
[15]R. F. Dashen, Phys. Rev. 134, A1025 (1964).
[16]M. Green, Proc. Phys. Soc. (London) 82, 204 (1963).
[17]D. B. Brown, DSc. thesis (MIT, 1965) (unpublished); *Quantitative Electron Probe Microanalysis*, Natl. Bur. Std. Spec. Publ. 298, 63 (1968); D. B. Brown and R. E. Ogilvie, J. Appl. Phys. 37, 4429 (1966).
[18]H. W. Streitwolf, Ann. Physik 3, 183 (1959).
[19]P. A. Wolff, Phys. Rev. 95, 56 (1954).
[20]J. Weymouth, Phys. Rev. 84, 766 (1951).
[21]D. B. Brown and R. E. Ogilvie, J. Appl. Phys. 35, 309 (1964).
[22]N. F. Mott and H. S. W. Massey, *The Theory of Atomic Collisions* (Oxford U. P., New York, 1949).
[23]R. D. Richtmyer and K. W. Morton, *Difference Methods for Initial Value Problems* (Interscience, New York, 1962).
[24]Higher-order corrections have been considered by G. I. Amelio and E. J. Scheibner, in *The Structure and Chemistry of Solid Surfaces*, edited by G. A. Somorjai (Wiley, New York, 1969),
[25]E. Jahnke and F. Emde, *Tables of Functions* (Dover, New York, 1945).
[26]See, for example, P. H. Cutler and J. C. Davis, Surface Sci. 1, 194 (1964).
[27]E. F. H. StG. Darlington, in *Fifth International Congress on X-Ray Optics and Microanalysis, Tubingen*, 1968, edited by G. Mollenstedt and K. H. Gaukler (Springer-Verlag, New York, 1969), p. 76.
[28]H. E. Biship, *X-Ray Optics and Microanalysis* (Hermann, Paris, 1966), p. 153.
[29]H. E. Bishop, Proc. Phys. Soc. (London) 85, 855 (1965).
[30]See, e.g., J. J. Quinn, Phys. Rev. 126, 1453 (1962).

PHYSICAL REVIEW B VOLUME 5, NUMBER 11 1 JUNE 1972

Analysis of the Fe^{3+}-V_O Center in the Tetragonal Phase of $SrTiO_3$

Th. von Waldkirch, K. A. Müller, and W. Berlinger
IBM Zurich Research Laboratory, 8803 *Rüschlikon, Switzerland*
(Received 3 January 1972)

The paramagnetic resonance spectrum of the iron oxygen-vacancy (Fe^{3+}-V_o) pair in the tetragonal $I4/mcm$ phase of $SrTiO_3$ at 78 °K is analyzed in detail. The spectra observed at K band are fully accounted for using the accepted structural properties of the crystal in the low-temperature phase. Whereas in the high-temperature cubic O_h^1 phase the Fe^{3+}-V_O spectra are axial, in the $D_{4h}^{18}-I4/mcm$ phase second-order perturbation terms of an orthorhombic $E(T)(S_x^2-S_y^2)$ term have to be taken into account with $E(T)=1.82\varphi^2(T)$ cm^{-1}, $\varphi(T)$ being the intrinsic rotational (order) parameter of the transition measured in radians. The analytically well understood spectrum justifies its use for the analysis of the structural phase transition observed in $SrTiO_3$ under applied stress and for the investigation of critical phenomena.

I. INTRODUCTION

In this paper a detailed analysis of the paramagnetic resonance spectrum of the Fe^{3+}-V_O center—a charge-compensated Fe^{3+} impurity—in strontium titanate at 78 °K is presented. The resonance of this center has been attributed to a three-valent-iron impurity substitutional for a Ti^{4+} ion with a nearest-neighbor oxygen vacancy, and analyzed previously in the cubic phase by Kirkpatrick, Müller, and Rubins,[1] hereafter referred to as KMR. The analysis consisted essentially of the Fe^{3+}-ground-state splitting in the presence of a large axial crystal-field term $D[S_z^2-\frac{1}{3}S(S+1)]$ with the z axis parallel to one of the three equivalent $\langle 100\rangle$ crystal axes. It has subsequently been refined by two groups by taking into account fourth-order terms in the spin Hamiltonian yielding agreement with the essential point of the KMR investigation.[2,3] Since then the center was also observed in $BaTiO_3$[4] and $KTaO_3$,[5] and the same kind of centers have now also been observed for other transition-metal ions such

as Ni^{3+}-V_O [6] and Co^{2+}-V_O [7] in $SrTiO_3$, and Co^{2+}-V_O [8] and Mn^{2+}-V_O [9] in $KTaO_3$. The Fe^{3+}-V_O center has recently proved to be extremely useful in the analysis of the behavior of $SrTiO_3$ below the cubic-to-tetragonal phase transition. The additional splitting of some resonance lines of the Fe^{3+}-V_O spectrum below the transition temperature $T_a = 105\,^\circ K$ has been measured as a function of temperature. Some of these splittings are directly proportional to the rotational order parameter $\varphi(T)$, [10, 11] others to the square of $\varphi(T)$. [12] The splittings proportional to $\varphi(T)$ yielded the temperature dependence of $\varphi(T)$ with a precision of about $\frac{1}{100}$ of an angular degree [13] due to the small linewidth of some 3 G and the large splitting value. For the same reasons these results are about a factor 2 to 3 more accurate than the ones obtained from the non-charge-compensated Fe^{3+}. As a function of uniaxial [111] stress the axis of the rotational motion $\vec{\varphi}$ deviates from the $\langle 100 \rangle$ axes. These deviations in terms of the $\langle 100 \rangle$ components and the magnitude of $\vec{\varphi}(T)$ were also obtained using the Fe^{3+}-V_O spectra and the onset of first- and second-order phase transitions to the trigonal $R\bar{3}c$ phase with [111] stress investigated below and above T_a. [14] The full analysis of the Fe^{3+}-V_O spectrum at a fixed temperature $T < T_a$ given here shows that its paramagnetic resonance data can be used for structural studies.

In Sec. II very detailed experiments on multi- and monodomain samples are reported from which an identification of all observed lines was possible. In Sec. III the theoretical analysis is presented extending the work of KMR and others [2, 3] by introduction of an orthorhombic term $E(S_x^2 - S_y^2)$ into the spin Hamiltonian and by use of the accepted structural properties of $SrTiO_3$ of alternately rotating octahedral units and c-axis elongation. The paper concludes with a discussion on the temperature dependences of the orthorhombic $E(T)$ term as well as the measured $\bar{\varphi}(T)$ rotation of the Fe^{3+}-V_O pair with respect to the intrinsic $\varphi(T)$ rotational parameter and the structural information obtainable by the Fe^{3+}-V_O resonance spectrum (Sec. IV).

II. EXPERIMENTAL RESULTS AND IDENTIFICATION OF RESONANCE LINES

The experiments were carried out with a superheterodyne single-side-band EPR spectrometer at K-band frequencies. The crystals were grown by the National Lead Co. using the Verneuil flame-fusion technique. To the powder feed 0.03-wt% Fe_2O_3 was added. In the cubic phase, besides the cubic spectrum of non-charge-compensated Fe^{3+}, [10, 11, 15] the resonance showed the strongly axial spectrum described and analyzed by KMR and others. [2, 3] At $T_a = 105\,^\circ K$, $SrTiO_3$ undergoes the cubic-to-tetragonal phase transition. Therefore, below T_a some of the resonance lines split due to the local lowering of symmetry and domain formation. Different domains are characterized by their tetragonal axes pointing in either of the three pseudocubic [100], [010], and [001] directions.

We used the same experimental arrangement as KMR, i.e., rotating the scanning magnetic field in a plane perpendicular to the cubic [001] crystal axis in the high-temperature phase. The first set of samples used were multidomain crystals usually cylindrical in shape with a diameter between 1 and 1.5 mm and 2–4 mm in length, the cylinder axis being parallel to a $\langle 100 \rangle$ direction. When the alignment between these crystals and the magnetic field is not exact within 0.1° then below T_a the *axial* resonance lines of the Fe^{3+}-V_O center split smoothly into a set of five lines. Figure 1 shows this resonance pattern at $g \sim 2$ for the magnetic field close to a pseudocubic [100] axis at 78 °K. If the crystals are aligned very carefully then two of the five lines collapse for all directions of the magnetic field in the (001) plane. The line which at high temperature appears isotropic at $g \sim 6$ splits into a set of three lines below T_a. In Fig. 2 the angular dependences of the lines for the magnetic field close to the [100] direction are depicted for both reso-

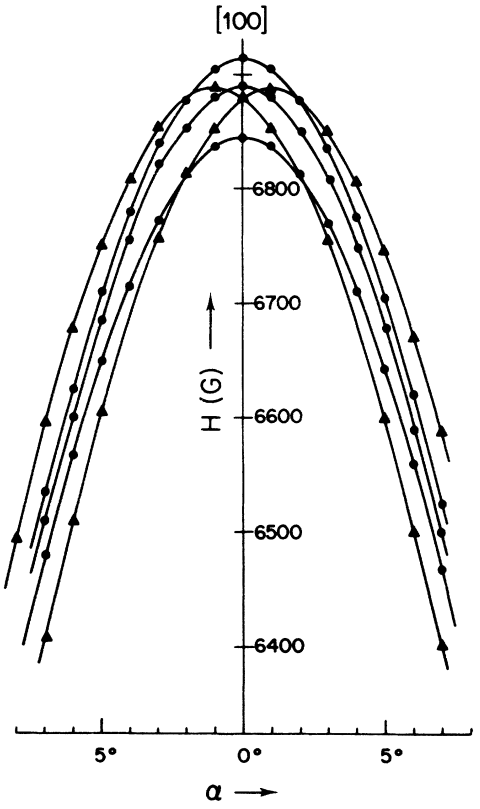

FIG. 1. High-field Fe^{3+}-V_O lines in a multidomain sample at 78 °K for a rotation of the magnetic field H in a pseudocubic (001) plane with improper alignment.

nances at $g \sim 2$ and $g \sim 6$. The doubly degenerate lines are indicated by boldface curves. The references are identification codes defined later. Figure 3 shows the resonance with the magnetic field around [110]. It appears that the angular behavior of three lines near $g \sim 2$ reported by Unoki and Sakudo[11] resulted from incomplete alignment of the crystals.

The split lines observed can be understood by considering the details of the cubic-to-tetragonal phase transition and the accepted microscopic structure of the pair center as proposed by KMR. The crystal transformation consists of alternate rotations of nearly rigid TiO_6 octahedra around Ti positions. Along the c axis consecutive (100) octahedral layers show alternate rotations as concluded by Unoki and Sakudo[11] from EPR Gd^{3+} data yielding a structure of $I4/mcm$. The rotation axis may be parallel to any of the three equivalent cube edges. In a macroscopic region of the crystal this is the tetragonal domain axis. The rotation angle φ, being the generalized order parameter of the transition,

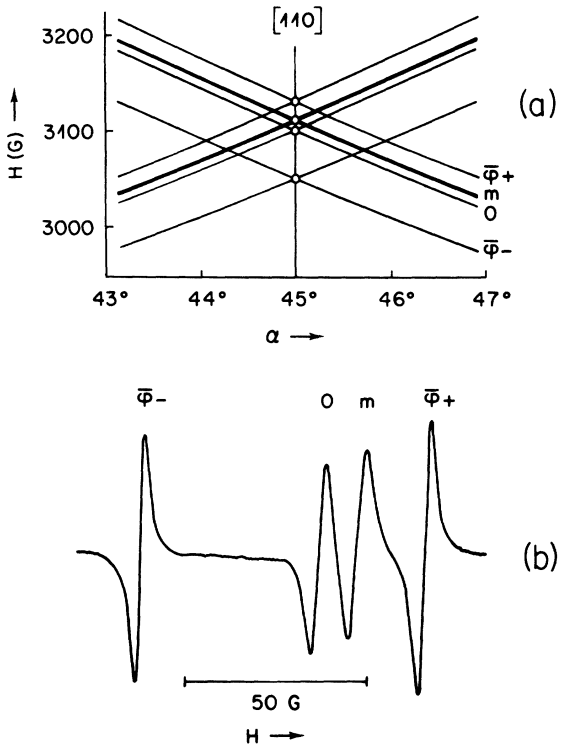

FIG. 3. Same resonances as in Fig. 2(a) for $\vec{H}$ near [110]. (a) Angular dependence of the resonance fields. (b) Resonance pattern with $\vec{H}$ parallel to [110].

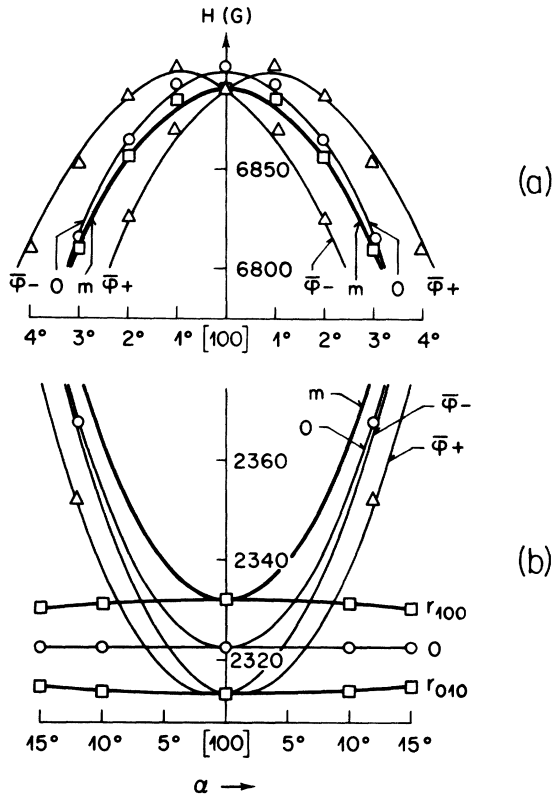

FIG. 2. Fe^{3+}-V_O resonances in a well-aligned multidomain sample with $\vec{H}$ in the pseudocubic (001) plane at 78 °K. (a) Experimental and theoretical angular dependence of the high-field resonances near [100]; (b) for low-field resonances ($g \sim 6$). Boldface lines indicate degenerate resonances.

is a function of temperature and for $T = 78$ °K has a value of $(1.53 \pm 0.05)°$ as determined from EPR spectra of Fe^{3+} ions in ordinary lattice positions (not charge compensated) (Fig. 4). For the Fe^{3+}-V_O center below T_a the missing oxygen ion can be located along the c axis of the domain or in the plane perpendicular to it. Figure 5 depicts schematically both cases showing some distortion around

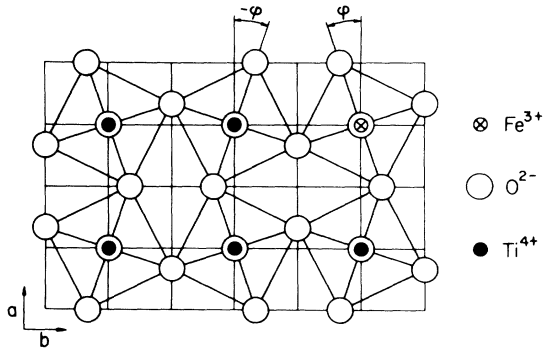

FIG. 4. Oxygen octahedra rotated around tetragonal c axis (domain axis) in $SrTiO_3$ below T_a. The presence of a non-charge-compensated Fe^{3+} substitutional impurity is indicated.

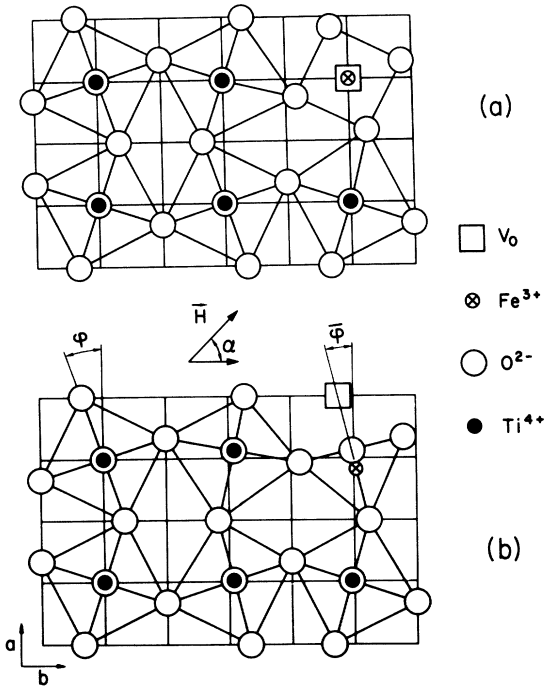

FIG. 5. Schematic representation of rotated and distorted oxygen octahedra near an Fe^{3+}-V_O pair for $T < T_a$. (a) Center axis parallel to rotation axis, yielding the axial O lines. (b) Center axis perpendicular to rotation axis. Situation for the orthorhombic spectra.

the Fe^{3+} due to relaxing neighbor ions from their ordinary positions. It is seen that the first type of centers remains axial, whereas for the second type, the transition-induced tetragonality is perpendicular to the main center axis, thus for these centers the transition causes a symmetry change from axial to orthorhombic.

For the first type of centers with their axes parallel to the domain axis the transition-induced tetragonality of the order of 10^{-3} cm^{-1} adds to the intrinsic large center axiality of 1.4 cm^{-1} (which is by itself temperature dependent). However, this small correction does not yield a measurable change in the effective g factor. Furthermore, the rotation of the oxygen complex occurs around the center axis and thus is not observable either. Therefore, the resonance positions of the Fe^{3+}-V_O pairs with their axis along the three possible domain axes are not affected by the phase transition, but correspond to the high-temperature lines analyzed by KMR. We call these lines zero lines (Figs. 2 and 3). The resonance fields of the split lines in the multidomain samples were checked with respect to these zero lines. In Fig. 6 the results for a rotation of the magnetic field parallel to a (001) plane are shown together with the theoretical curves as described in Sec. III. Figure 7 shows the splittings between the zero and the other lines.

In order to identify the split lines resulting from the *orthorhombic* centers samples were used which

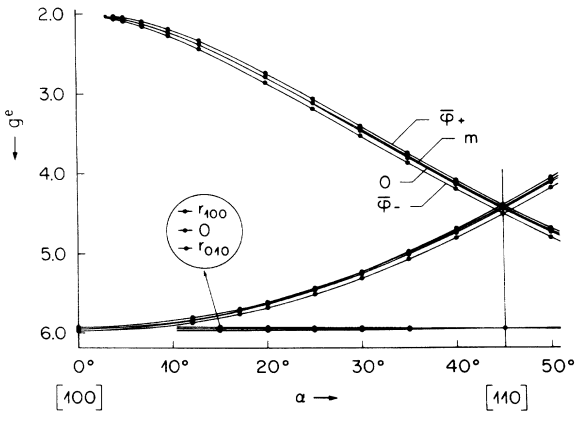

FIG. 6. Experimental data and theoretical curves of the Fe^{3+}-V_O resonances in strontium titanate at 78°K for a rotation of the magnetic field in a pseudocubic (001) plane of the crystal at a microwave frequency of 19.34 GHz.

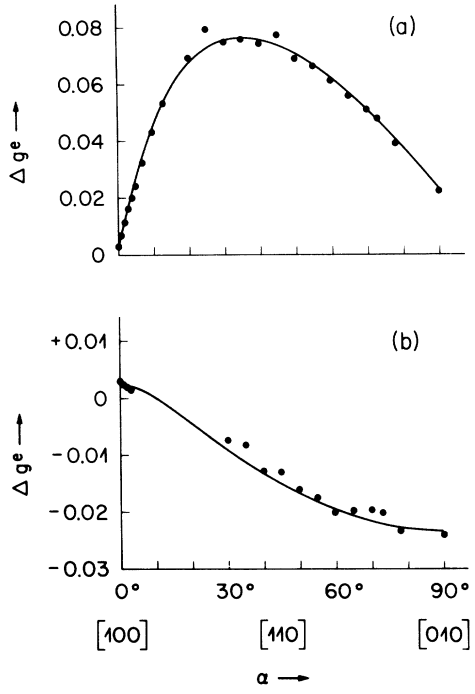

FIG. 7. Differences of the effective g factor between the orthorhombic and the corresponding axial lines as a function of magnetic field direction within the pseudocubic (001) plane (a) for the $\bar{\varphi}_-$ lines, (b) for the m lines. Between $\alpha = 5°$ and 25° the orthorhombic m and axial O lines are not resolved. Solid lines represent the theoretical curves.

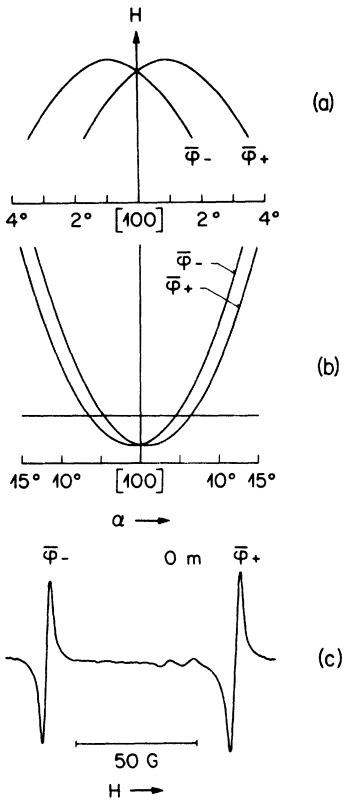

FIG. 8. Similar data as in Figs. 2 and 3(b), but measured in a monodomain sample with domain axis parallel to the pseudocubic [001] direction. These results were used for the identification of the lines.

below T_a transform into a *monodomain* crystal. Two methods have been developed to achieve this.[16] The first consists of machining flat rectangular (110) plates thinner than 0.3 mm. The larger basis of such a plate is parallel to a [001] direction and typically 7 mm long, the other basis is parallel to a $[1\bar{1}0]$ edge. Below T_a such a sample transforms into a {001} monodomain, where the symbol {001} denotes a domain with c axis parallel to the [001] direction. In the second method uniaxial [110] stress is applied to a thick sample which for sufficiently high pressures (~1 kg/mm^2) becomes near monodomain along {001}. If stress along a [001] direction is applied the sample consists of {100} and {010} domains. All these effects result from the fact that the c/a ratio is larger than unity.[17]

The thin samples obtained by shaping are inherently strained along the [110] direction due to the grinding of the surfaces. This strain causes the monodomain effect, and has recently been found to fade away in the course of some months. It also disappeared by annealing the samples for 6 h at 1550 °C. In the present experiments such (110) flat plates were aligned with their {001} monodomain axis parallel to the rotation axis of the magnet, i.e., $\vec{H}$ lies in the tetragonal (001) plane. For further identification of resonance lines flat (001) plates containing {100} and {010} domains due to their "built-in" strain were also used, aligned with their (001) plane parallel to the magnetic field plane.

For a monodomain {001} sample with $\vec{H}$ rotating in the (001) plane, the resonance pattern as shown in Fig. 8 was observed [compare Figs. 2 and 3(b)]. The zero line at $g \sim 6$ results from the *axial* Fe^{3+}-V_O pairs parallel to the {001} domain axis. The lines denoted by $\bar{\varphi}_+$ and $\bar{\varphi}_-$ belong to *orthorhombic* Fe^{3+}-V_O pairs in the (001) plane, rotated by $\pm\bar{\varphi}$ away from the respective a axis as indicated for one center in Fig. 5(b). In the region near $g \sim 2$ these two spectra $\bar{\varphi}_+$ and $\bar{\varphi}_-$ correspond to pairs located in two inequivalent octahedral sublattices rotated against each other by 2φ. They are clearly resolved near $g \sim 2$, whereas in the region near $g \sim 6$ this is not the case due to the weaker dependence of the resonance field strength on field direction. Due to the presence of the oxygen vacancy and the resulting local distortion of the oxygen pyramid around the Fe^{3+} ion, $\bar{\varphi}$ is smaller than φ and at 78 °K was determined to be $\bar{\varphi} = (0.95 \pm 0.05)°$[14] [Fig. 5(b)]. We note that for $\vec{H}$ parallel to the pair axis the orthorhombicity does not enter. Thus, the maximum of the resonance field for $\bar{\varphi}_+$ and $\bar{\varphi}_-$ is the same as for the zero line at $g = 2.0037$ [see Fig. 2(a)], whereas near $g \sim 6$, where $\vec{H}$ is perpendicular to the pair axis, the orthorhombicity causes a shift to lower fields with respect to the corresponding zero line [Fig. 8(b)]. For $\vec{H}$ parallel to [110] the $\bar{\varphi}_+$ and $\bar{\varphi}_-$ lines are the two outmost ones [Fig. 8(c)].

After the identification of the zero, $\bar{\varphi}_+$, and $\bar{\varphi}_-$ lines, the origins of the remaining lines in the multidomain resonance pattern (Figs. 2 and 3) are easily recognized. They result from Fe^{3+}-V_O pairs located in {100} and {010} domains. This was verified by using thin (001) plates which, due to their "built-in" [001] strain, contained only {100} and {010} domains. For these measurements $\vec{H}$ was rotated in the (001) plate plane. The axial zero lines again result from centers parallel to the domain axes. Near $g \sim 2$ [see Fig. 2(a)] the line denoted by m for "mirror" is due to centers with axes tilted by $\pm\bar{\varphi}$ out of the (001) plane. For these centers the (001) plane is a mirror plane, therefore they yield one degenerate line for $\vec{H}$ in the (001) plane. Near $g \sim 2$, where $\vec{H}$ is nearly parallel to the center and hence the orthorhombicity does not enter significantly, the difference between the maximum of the magnetic resonance fields of the m line and the zero line is entirely due to the inclination of the centers by $\pm\bar{\varphi}$ with respect to the magnetic field. In the region near $g \sim 6$ two lines are

observed. They are due to Fe^{3+}-V_O pairs with their axes tilted by an angle $\bar{\varphi}$ from the [001] direction. The tilt is either $\pm\bar{\varphi}$ towards the [100] direction for centers in a {010} domain or $\pm\bar{\varphi}$ towards the [010] direction for those in a {100} domain. Within one domain, the centers tilted by $\pm\bar{\varphi}$ are again degenerate as they are related to one another by the inversion operation and the (001) mirror plane. Therefore the two orthorhombic lines at $g \sim 6$, denoted by r_{100} and r_{010} ["rhombic," Fig. 2(b)] are again doubly degenerate and correspond to centers belonging to {100} or {010} domains and tilted by $\pm\bar{\varphi}$ away from the [001] direction. It may be noted that in this case where $\vec{H}$ is nearly perpendicular to the center axis the difference between r_{100} and r_{010} and the corresponding zero line is essentially due to the orthorhombicity, since the effect of the inclination is negligible as demonstrated by the collapsing of the $\bar{\varphi}_+$ and $\bar{\varphi}_-$ lines near $g \sim 6$.

III. THEORETICAL ANALYSIS

As discussed in Sec. II, the resonance lines of the Fe^{3+}-V_O center observed can be divided into two groups: those resulting from centers with axes parallel to the domain axis and those with their axes perpendicular to it. The former centers see an axial local symmetry and are thus analyzed by the axial spin Hamiltonian used earlier.[1-3] For the second group, the local symmetry is orthorhombic which requires an extension of the axial Hamiltonian to include orthorhombic crystal-field and Zeeman terms. Calling the main center axis z and taking it as axis of quantization, $\mathcal{H}$ may be written

$$\mathcal{H} = \tfrac{1}{3}D\,O_2^0 + \tfrac{1}{180}F\,O_4^0 + \tfrac{1}{120}a(O_4^0 + 5O_4^4) + EO_2^2 + G_z H_z S_z + G_x H_x S_x + G_y H_y S_y \,, \quad (1)$$

with $G_i = \mu_B g_i$ (μ_B = Bohr magneton) and the usual definitions of the O_l^m operators.[18] Using θ and δ as the polar angles of the magnetic field with respect to the main axis z of the local center, (1) is reexpressed in terms of the spin operators S_z, $S_\pm = S_x \pm iS_y$:

$$\mathcal{H} = D(S_z^2 - \tfrac{1}{4}) + \tfrac{1}{180}F\left[35S_z^4 - 30S(S+1)S_z^2 + 25S_z^2 + \tfrac{915}{16}\right] + \tfrac{1}{120}a\left[35S_z^4 - 30S(S+1)S_z^2 + 25S_z^2 + \tfrac{915}{16} + \tfrac{5}{2}(S_+^4 + S_-^4)\right] + \tfrac{1}{2}E(S_+^2 + S_-^2) + \mu_B H\left[g_z S_z \cos\theta + \tfrac{1}{2}g_x(S_+ + S_-)\sin\theta\cos\delta - \tfrac{1}{2}ig_y(S_+ - S_-)\sin\theta\sin\delta\right] . \quad (2)$$

It should be noted that in (2) the constants $\frac{8}{3}D$, $-\frac{2}{3}F$, and $-a$ have been added to the first three terms of (1) in order to yield a zero shift for the magnetic $\pm\frac{1}{2}$ doublet for which the resonance transitions are observed. This simplifies the calculations.

Comparison of the results obtained in the high-temperature phase by perturbation calculation[1] and by direct computer diagonalization of the $S = \frac{5}{2}$ matrix[3] yielded a negligible error of 0.004% at X band, where $h\nu$ is of the order of 25% of the crystal-field energy $|2D|$. Henderson *et al.*[19] determined the g tensor and the crystal-field parameters for the case of charge-compensated Fe^{3+} in MgO by both methods with $h\nu$ of the order of 70% of $|2D|$, finding again negligible errors caused by perturbation calculation. Therefore, it is correct to proceed by perturbation theory in our case, too, where $h\nu/|2D|$ is smaller than 50%.

The first two terms in (2) are taken as zero-order Hamiltonian $\mathcal{H}_0$ and the other crystal-field terms and the Zeeman splittings are treated as perturbation $\mathcal{H}_1$. In terms of the magnetic eigenstates $S_z = |\pm\frac{5}{2}\rangle$, $|\pm\frac{3}{2}\rangle$, and $|\pm\frac{1}{2}\rangle$ the matrix of $\mathcal{H}_0$ is then diagonal with the eigenvalues $6D - \frac{1}{3}F$, $2D - \frac{5}{3}F$, and 0, respectively. The matrix of the perturbation Hamiltonian on the same basis is given by

$\mathcal{H}_1$	$\lvert\frac{5}{2}\rangle$	$\lvert\frac{3}{2}\rangle$	$\lvert\frac{1}{2}\rangle$	$\lvert-\frac{1}{2}\rangle$	$\lvert-\frac{3}{2}\rangle$	$\lvert-\frac{5}{2}\rangle$
$\langle\frac{5}{2}\rvert$	$5A - \frac{1}{2}a$	$\sqrt{(\frac{5}{9})}B^*$	$\sqrt{(10)}E$	0	$\sqrt{(\frac{5}{4})}a$	0
$\langle\frac{3}{2}\rvert$	$\sqrt{(\frac{5}{9})}B$	$3A - \frac{5}{2}a$	$\sqrt{(\frac{8}{9})}B^*$	$\sqrt{(18)}E$	0	$\sqrt{(\frac{5}{4})}a$
$\langle\frac{1}{2}\rvert$	$\sqrt{(10)}E$	$\sqrt{(\frac{8}{9})}B$	A	B^*	$\sqrt{(18)}E$	0
$\langle-\frac{1}{2}\rvert$	0	$\sqrt{(18)}E$	B	$-A$	$\sqrt{(\frac{8}{9})}B^*$	$\sqrt{(10)}E$
$\langle-\frac{3}{2}\rvert$	$\sqrt{(\frac{5}{4})}a$	0	$\sqrt{(18)}E$	$\sqrt{(\frac{8}{9})}B$	$-3A - \frac{5}{2}a$	$\sqrt{(\frac{5}{9})}B^*$
$\langle-\frac{5}{2}\rvert$	0	$\sqrt{(\frac{5}{4})}a$	0	$\sqrt{(10)}E$	$\sqrt{(\frac{5}{9})}B$	$-5A - \frac{1}{2}a$

with

$$A = \tfrac{1}{2}g_z\mu_B H\cos\theta \,,$$

$$B = \tfrac{3}{2}\mu_B H\sin\theta(g_x\cos\delta + ig_y\sin\delta) \,,$$

$$B^* = \tfrac{3}{2}\mu_B H\sin\theta(g_x\cos\delta - ig_y\sin\delta) \,,$$

and

$$\mu_B = \text{Bohr magneton.} \tag{3}$$

Since the eigenvalues of $\mathcal{H}_0$ are doubly degenerate and $\mathcal{H}_1$ couples via B and B^* between eigenstates within the same eigenspace with energy zero, the basis of this eigenspace has first to be adapted to the perturbation such that the submatrix of $\mathcal{H}_1$ within this eigenspace $|\pm\frac{1}{2}\rangle$ becomes diagonal. This diagonalization, carried out by KMR for real B's only, in our case of complex B terms leads to the following complex eigenfunctions $|\gamma\rangle$ and $|\delta\rangle$:

$$|\gamma\rangle = \alpha|\tfrac{1}{2}\rangle + \beta|-\tfrac{1}{2}\rangle ,$$

$$|\delta\rangle = -\beta|\tfrac{1}{2}\rangle + \alpha^*|-\tfrac{1}{2}\rangle ,$$

$$\alpha = \left(\frac{B^*}{B}\right)^{1/2}\left(\frac{(A^2+|B|^2)^{1/2}+A}{2(A^2+|B|^2)^{1/2}}\right)^{1/2} , \tag{4}$$

$$\beta = \left(\frac{(A^2+|B|^2)^{1/2}-A}{2(A^2+|B|^2)^{1/2}}\right)^{1/2} ,$$

and the eigenvalues

$$W_{\gamma,\delta} = \pm(A^2+|B|^2)^{1/2} .$$

Note that due to the complex quantity B, α differs by a phase factor $(B^*/B)^{1/2}$ from that in Eq. (2) of KMR. The above matrix transforms within the new basis:

$\mathcal{H}_1$	$\lvert\frac{5}{2}\rangle$	$\lvert\frac{3}{2}\rangle$	$\lvert\gamma\rangle$	$\lvert\delta\rangle$	$\lvert-\frac{3}{2}\rangle$	$\lvert-\frac{5}{2}\rangle$
$\langle\frac{5}{2}\rvert$	$5A-\frac{1}{2}a$	$\sqrt{(\frac{5}{9})}B^*$	$\alpha\sqrt{(10)}E$	$-\beta\sqrt{(10)}E$	$\sqrt{(\frac{5}{4})}a$	0
$\langle\frac{3}{2}\rvert$	$\sqrt{(\frac{5}{9})}B$	$3A-\frac{5}{2}a$	$\alpha\sqrt{(\frac{8}{9})}B^*+\beta\sqrt{(18)}E$	$\alpha^*\sqrt{(18)}E-\beta\sqrt{(\frac{8}{9})}B^*$	0	$\sqrt{(\frac{5}{4})}a$
$\langle\gamma\rvert$	$\alpha^*\sqrt{(10)}E$	$\alpha^*\sqrt{(\frac{8}{9})}B+\beta\sqrt{(18)}E$	$(A^2+\lvert B\rvert^2)^{1/2}$	0	$\alpha^*\sqrt{(18)}E+\beta\sqrt{(\frac{8}{9})}B^*$	$\beta\sqrt{(10)}E$
$\langle\delta\rvert$	$-\beta\sqrt{(10)}E$	$\alpha\sqrt{(18)}E-\beta\sqrt{(\frac{8}{9})}B$	0	$-(A^2+\lvert B\rvert^2)^{1/2}$	$\alpha\sqrt{(\frac{8}{9})}B^*-\beta\sqrt{(18)}E$	$\alpha\sqrt{(10)}E$
$\langle-\frac{3}{2}\rvert$	$\sqrt{(\frac{5}{4})}a$	0	$\alpha\sqrt{(18)}E+\beta\sqrt{(\frac{8}{9})}B$	$\alpha^*\sqrt{(\frac{8}{9})}B-\beta\sqrt{(18)}E$	$-3A-\frac{5}{2}a$	$\sqrt{(\frac{5}{9})}B^*$
$\langle-\frac{5}{2}\rvert$	0	$\sqrt{(\frac{5}{4})}a$	$\beta\sqrt{(10)}E$	$\alpha^*\sqrt{(10)}E$	$\sqrt{(\frac{5}{9})}B$	$-5A-\frac{1}{2}a$

If E differs from zero, second-order perturbation terms split the $|\gamma\rangle$ and $|\delta\rangle$ levels further, whereas in the work by KMR, $E=0$. The additional split is only caused by the admixture of $|\pm\frac{3}{2}\rangle$ levels into the ground states $|\gamma\rangle$ and $|\delta\rangle$ and is given by

$$\begin{aligned}\Delta W_\gamma^{(2)} - \Delta W_\delta^{(2)} &= -\frac{8}{D'}\,\beta E(\alpha B^* + \alpha^* B)\\ &= -\frac{4E}{D'}\,\frac{BB+B^*B^*}{(A^2+B^*B)^{1/2}}\\ &= -\frac{36E}{D'}\,\mu_B H\sin^2\theta\\ &\times\frac{g_x^2\cos^2\delta - g_y^2\sin^2\delta}{[g_z^2\cos^2\theta + 9\sin^2\theta(g_x^2\cos^2\delta + g_y^2\sin^2\delta)]^{1/2}} ,\end{aligned} \tag{5}$$

with $2D' = 2D - \frac{5}{3}F$. In third-order perturbation $\Delta W_\gamma^{(3)}$ and $\Delta W_\delta^{(3)}$ have been fully evaluated[20]:

$$\begin{aligned}\Delta W_\gamma^{(3)} &= \sum_{m\neq\gamma,\delta}\frac{|\mathcal{H}_{\gamma m}|^2}{(E_m - E_\gamma)^2}(\mathcal{H}_{mm} - \mathcal{H}_{\gamma\gamma})\\ &+ \sum_{m\neq\gamma,\delta}\sum_{p\neq m,\gamma,\delta}\frac{\mathcal{H}_{mp}\mathcal{H}_{p\gamma}}{(E_\gamma - E_p)(E_\gamma - E_m)} .\end{aligned} \tag{6}$$

Considering only terms which contribute to the splitting of the $|\gamma\rangle$ and $|\delta\rangle$ levels the first term yields numerators proportional to $A|B|^2$, $|B|^2 \times (A^2+|B|^2)^{1/2}$, aEB, aEB^*, and $E^2(A^2+|B|^2)^{1/2}$ divided by $(2D')^2$ and $(6D-\frac{1}{3}F)^2$, respectively. The second term in (6) not considered by KMR gives numerators proportional to BE^2, B^*E^2, and aBE, aB^*E divided by terms of the order of $12D^2$.

From these third-order splittings we retain only those which are cubic in the Zeeman terms A, B, and B^*, since the Zeeman energy is of the order of 1 cm^{-1} at K band, whereas a and E are of the order of 10^{-2} and 10^{-3} cm^{-1}, respectively. Within this approximation the terms which couple between the $|\pm\frac{5}{2}\rangle$ levels and the ground states do not contribute. Therefore, the same result is obtained by perturbation calculation starting from the $|\pm\frac{3}{2}\rangle$, $|\pm\frac{1}{2}\rangle$ submatrix only, as in KMR. In this case we may incorporate the cubic a-field term, which within these substates is diagonal, into the unperturbed Hamiltonian $\mathcal{H}_0$. The eigenstates of H_0 are then $(2D-\frac{5}{2}a-\frac{5}{3}F)$ and zero for the $|\pm\frac{3}{2}\rangle$, $|\pm\frac{1}{2}\rangle$ doublets, respectively, and for the axial case treated by KMR we obtain the result quoted by Baer *et al.*,[2] Pontin *et al.*,[3] and Henderson *et al.*[19]

The general expression for the experimental g value g^e[1] in the orthorhombic case is now given by

$$\begin{aligned}g^e = (g_z^2\cos^2\theta + 9g_\perp^2\sin^2\theta)^{1/2}&\left(1 - \frac{2(g_\perp\mu_B H)^2}{(2D'')^2}\,F(\theta)\right)\\ &- \frac{36E}{D''}\sin^2\theta\,\frac{g_x^2\cos^2\delta - g_y^2\sin^2\delta}{(g_z^2\cos^2\theta + 9g_\perp^2\sin^2\theta)^{1/2}} ,\end{aligned} \tag{7}$$

where

$$g_\perp^2 = g_x^2\cos^2\delta + g_y^2\sin^2\delta ,$$

$$2D'' = 2D - \tfrac{5}{2}a - \tfrac{5}{3}F ,$$

$$F(\theta) = \sin^2\theta\left(\frac{(9g_\perp^2 + 2g_z^2)\sin^2\theta - 2g_z^2}{(9g_\perp^2 - g_z^2)\sin^2\theta + g_z^2}\right) .$$

The reference axes of the polar angles θ and δ of the magnetic field coincide with the local main center axis which has C_{2v} symmetry, and with the local domain axis, respectively (see Fig. 5). As shown in Sec. II, below the phase transition the different Fe^{3+}-V_O centers in the crystal are tilted in a different manner with respect to the magnetic field according to the direction of their axes in the high-temperature phase and to the local domain axis, yielding the lines O, $\bar{\varphi}_+$, $\bar{\varphi}_-$, m, r_{100}, and r_{010}. Thus, θ and δ have to be evaluated for each of the lines. For the magnetic field in the pseudocubic (001) plane they are given in Table I.

Equation (7) was numerically evaluated for the five spectra at 78 °K on an IBM 1130 computer using a 2250 display unit with $\bar{\varphi} = 0.95°$.[14] $g_{\parallel}^{e} = g_{\parallel}$ was found to be 2.0037 ± 0.0015, which is a little smaller than the high-temperature value found by KMR, but is equal to the value of the non-charge-compensated Fe^{3+}. This quantity is very sensitive to misalignment of the sample, being easily shifted to higher values. The difference between our $g_{\parallel}$ and the one found by KMR would imply a misalignment there of less than 0.8°. Assuming the g tensor to remain axial (see Sec. IV) and using $g_x \doteq g_y = g_\perp = 2.010$ obtained by KMR in the high-temperature phase by measuring at two different frequencies, the best fit to the experimental points was achieved using the following values for $|2D''|$ and $|E|$:

$$|2D''| = 2.70 \pm 0.03 \text{ cm}^{-1},$$

$$|E| = (1.295 \pm 0.015) \times 10^{-3} \text{ cm}^{-1}$$

(for the orthorhombic centers).

The value of $|2D''|$ is in good agreement with the high-temperature values reported by KMR, Baer *et al.*,[2] and Pontin *et al.*,[3] indicating that $|2D''|$ is little temperature dependent. The calculated curves are depicted in Figs. 2, 3, and 6. The theory fits the experimental curves everywhere within approximately 0.3%. For the evaluation of the orthorhombicity E/D'' it is preferable to check the theory for the *differences* between the orthorhombic and the corresponding axial spectra O, as done in Fig. 7, since then errors in the angular dependence of g^e due to neglection of higher-order Zeeman-perturbation terms tend to cancel. In Fig. 7(b), for α between 5° and 25° the two resonance lines are so close together that they are not resolved.

The good agreement between theory and experiment demonstrated by Figs. 2, 6, and 7 shows that the splittings of the Fe^{3+}-V_O resonances below the phase-transition temperature are well understood, and indicates that the approximations made in the third-order perturbation calculation are justified.

IV. DISCUSSION

A. Rotational Parameter $\bar{\varphi}(T)$

The rotation angle $\bar{\varphi}(T)$ of the oxygen complex around a charge-compensated Fe^{3+} ion is somewhat smaller than the intrinsic rotation angle $\varphi(T)$ due to the distortion of the lattice by the missing oxygen ion (Fig. 5). Both quantities were measured directly. They were found to be proportional to each other between 30 and 85 °K. In this range the proportionality is given by[14]

TABLE I. Direction of tilt of Fe^{3+}-V_O center. α is the angle of the magnetic field with respect to the pseudocubic [100] direction.

Domain axis \ Center axis in high-temperature phase	[100]	[010]	[001]
[100]	$\cos\theta = \cos\alpha$ O	$\cos\theta = \cos\bar{\varphi}\sin\alpha$ $\cos\delta = \frac{\cos\alpha}{\sin\theta}$ m	$\cos\theta = \sin\bar{\varphi}\sin\alpha$ $\cos\delta = \frac{\cos\alpha}{\sin\theta}$ r_{100}
[010]	$\cos\theta = \cos\bar{\varphi}\cos\alpha$ $\cos\delta = \frac{\sin\alpha}{\sin\theta}$ m	$\cos\theta = \sin\alpha$ O	$\cos\theta = \sin\bar{\varphi}\cos\alpha$ $\cos\delta = \frac{\sin\alpha}{\sin\theta}$ r_{010}
[001]	$\cos\theta = \cos(\alpha \pm \bar{\varphi})$ $\cos\delta = 0$ $\bar{\varphi}_\pm$	$\cos\theta = \sin(\alpha \pm \bar{\varphi})$ $\cos\delta = 0$ $\bar{\varphi}_\pm$	$\cos\theta = 0$ O

$$\varphi(T) = (1.59 \pm 0.05)\,\bar{\varphi}(T) \ .$$

Small deviations from proportionality occur at lower temperatures. Due to the narrow width of the Fe^{3+}-V_O lines of 1.3 G for H parallel [100] at $g \sim 6$ and 2.7 G for the high-field line at 78 °K and the large splitting caused by $\bar{\varphi}(T)$ (the difference between spectra $\bar{\varphi}_+$ and $\bar{\varphi}_-$ is 81 G at 78 °K) the center may therefore be used as a sensitive monitor of the order-parameter $\varphi(T)$ near the phase-transition T_a.

B. Orthorhombic $E(T)$ Term

As seen from Sec. III, the present analysis was done assuming an orthorhombic crystal-field term together with the axial g tensor measured above the phase transition. Essentially, the same results, however, could be obtained using both an orthorhombic g factor and an orthorhombic crystal-field term or even an orthorhombic g tensor alone. In principle, experiments at two different microwave frequencies are required to distinguish properly between these two cases, as done for the high-temperature phase by KMR.[1] Differences between both cases manifest themselves by mixed terms between Zeeman and crystal-field energy in third-order perturbation. In our case, however, these third-order terms are too small to be measured by experiments at two frequencies.

Our assumption of an orthorhombic crystal-field term $E(T)(S_x^2 - S_y^2)$ without change in the axial g tensor is based on the following arguments:

(i) In the high-temperature phase where the Fe^{3+}-V_O center is strongly axial, KMR found the g tensor to be nearly isotropic with an axiality of less than 0.5% despite the very high local axial crystal field $D = 1.4\ \mathrm{cm}^{-1}$. A significant change in the g tensor would therefore not be readily explainable by the very small structural change caused by the phase transition, which yields for the non-charge-compensated Fe^{3+} center a maximum axial D term of only $1.1 \times 10^{-3}\ \mathrm{cm}^{-1}$ at 4.2 °K.[11]

(ii) The temperature dependence of the rhombic splitting of the Fe^{3+}-V_O resonances (see Fig. 2 of Ref. 10) is proportional to the square of the rotational parameter $\bar{\varphi}^2(T)$ (Fig. 3 of Ref. 12). If we assume $2D'' = 2D - \frac{5}{2}a - \frac{5}{3}F$ to be constant with temperature compared to the orthorhombic $E(T)$ term, then the temperature dependence of the rhombic splitting is directly proportional to that of $E(T)$ [Eq. (7)]. Due to the C_{2v} symmetry of the center $E \propto (c/a - 1) \propto \varphi^2$, we then have

$$E(T) = \rho\,\varphi^2(T) \ ,$$

with

$$\rho = 1.82 \pm 0.08\ \mathrm{cm}^{-1}\ \mathrm{rad}^{-2} \ .$$

Therefore $E(T)$ follows the same temperature dependence as the axial crystal-field term $D(T)$ of the non-charge-compensated Fe^{3+} ion.[10-12] Furthermore, the size of $E(T)_{Fe^{3+}\text{-}V_O}$ is also of the same order of magnitude as $D(T)_{Fe^{3+}}$, e.g., at 78 °K, $E(T) = 13 \times 10^{-4}\ \mathrm{cm}^{-1}$ and $D(T) = 6.3 \times 10^{-4}\ \mathrm{cm}^{-1}$.[11] If the deformation of the oxygen complexes around the Fe^{3+} ions resulting from the phase transition were equal for both cases, these two quantities should be related by $2E_{Fe^{3+}\text{-}V_O} = D_{Fe^{3+}}$. The observed value of $2E_{Fe^{3+}\text{-}V_O}/D_{Fe^{3+}} = 4.1$ therefore indicates that the vacancy complex gets somewhat more distorted than the regular octahedron. As pointed out by Alefeld[17] the c/a ratio of the rotated oxygen octahedra is given by the difference of a axis elongation due to the oxygen ions moving along a pseudocubic ⟨100⟩ direction and intrinsic c-axis elongation. Thus, assuming the same intrinsic c-axis elongation for both centers, the difference in rotational parameter would yield a $1.59^2 = 2.5$ times larger net elongation of the vacancy complex. The remaining difference to obtain 4.1 probably results from lattice or oxygen-electron-cloud distortion by the missing oxygen ion.

C. Application of the Center for Structural Studies

As pointed out, the Fe^{3+}-V_O center provides a sensitive tool for studying small structural rotational changes in the crystal. The highest sensitivity of the resonance fields with respect to angular changes and therefore best accuracy for experimental g factors is achieved in the range of θ between 10° and 30°, where θ is the angle of the magnetic field with respect to the center axis. This may easily be visualized by transforming the $g^e(\theta)$ curve of Fig. 6 to the analogous magnetic field curve. For many applications, however, the region near [110] is preferable, since here all different domain resonances are resolved, besides a practically optimal angular dependence, and the linewidth is somewhat narrower. Furthermore, exact alignment is here easily reproducible since at [110] the resonances of two mutually perpendicular centers coincide (Figs. 3 and 6). Near [100] and $g \sim 2$, on the other hand, overlap with the strong $\pm\frac{1}{2}$ Fe^{3+} line is often disturbing.

The splittings of the Fe^{3+}-V_O pair lines have been used recently in an investigation of $SrTiO_3$ under uniaxial [111] stress.[14] Above a critical stress p_c, $SrTiO_3$ undergoes a phase transition to a trigonal ($R\bar{3}c$) phase in which the octahedra rotate alternately around a pseudocubic body diagonal. For $T < T_a$ the transition is first order in character, whereas for $T > T_a$ it is second order. The variable temperature cryostat allowed the application of stress only perpendicular to the external magnetic field H. Under this geometry the EPR spectrum of Fe^{3+} substitutional for Ti^{4+} is insensitive to the octahedral rotation $\vec{\varphi}$ in the trigonal

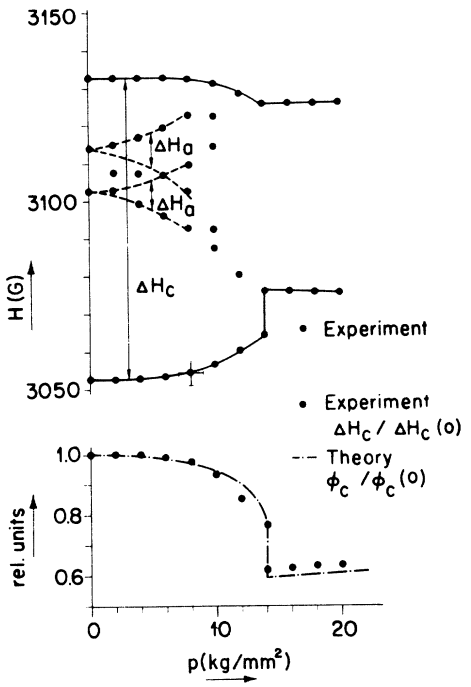

FIG. 9. Experimental and theoretical line shift of the Fe^{3+}-V_O resonances for stress p parallel to a pseudocubic [111] direction and $\vec{H} \parallel [1\bar{1}0]$ at 78 °K (taken from Ref. 14). The shifts and splittings result from the change in direction of the rotational axis (see text).

phase. From the present analysis we see that for $\vec{H} \parallel [1\bar{1}0]$ the splitting of the $\bar{\varphi}_+$ and $\bar{\varphi}_-$ lines resulting from a {001} domain is given according to Eq. (7),

$$\Delta H_c = H(\bar{\varphi}_{+c}) - H(\bar{\varphi}_{-c}) = 42.5(\bar{\varphi}_{+c} - \bar{\varphi}_{-c}) = 85\,|\,\bar{\varphi}_c|\ ,$$

where $\bar{\varphi}_c$ is the component of rotation parallel to the [001] pseudocubic direction (c axis of the domain) measured in angular degrees. Figure 9 shows the variation of the EPR lines with [111] stress for H parallel to a $[1\bar{1}0]$ pseudocubic direction at 78 °K. It is seen that ΔH_c, i.e., the $\bar{\varphi}_c$ component decreases because $\vec{\varphi}$ is tilted away from the c axis towards [111]. Similar behavior occurs for the {100} and {010} domains, where $\vec{\varphi}$ is also tilted towards [111]. Therefore, the pair centers within these domains become inequivalent due to the loss of mirror symmetry caused by rotation towards and away from $\vec{H}$ by proportionate amounts. This effect splits the O and m lines by an amount ΔH_a indicated in Fig. 9. ΔH_a here is proportional to the $\bar{\varphi}_{001}$ components of $\vec{\varphi}$ in the {100} and {010} domains.

Above p_c the spectrum collapses into a pair of slowly varying degenerate lines resulting from $\pm\varphi$ rotations around the [111] direction parallel to stress. The crystal now consists of a trigonal monodomain. We note that just above p_c, $\Delta H_c(p_c) = (1/\sqrt{3})\,\Delta H_c(0)$ (see Fig. 9). This means that within the experimental accuracy $|\vec{\varphi}|$ (i.e., the magnitude of the rotation) is constant but the direction has rotated from the equivalent ⟨100⟩ directions into $[111] \parallel \vec{p}_c$. For $T < T_a$ this change occurs discontinuously (Fig. 9) and for $T > T_a$ continuously, as discussed and analyzed in detail in Ref. 14, where the phase boundaries have been determined over an extended temperature range.

The Fe^{3+}-V_O pair center lines have more recently also been employed to study the critical behavior of the cubic-to-tetragonal phase transition at 105 °K.[13] As mentioned in Sec. I, the large splitting for small rotation angle allowed the determination of the temperature dependence for the rotational parameter $\varphi(T)$ close to T_a, hence of the static critical exponent β of the transition. A recent analysis yielded $\beta = 0.333 \pm 0.010$.[13] Near T_a, φ fluctuates: $\varphi = \langle\varphi(T)\rangle + \delta\varphi$. This causes a broadening of the $\bar{\varphi}_+$ and $\bar{\varphi}_-$ lines for T approaching T_a from above ($\bar{\varphi}_+ \equiv \bar{\varphi}_-$) and below. This broadening, due to the *local* fluctuations, has been reported recently[21] and considered theoretically by Schwabl.[22] More accurate very recent experimental results and a theoretical analysis including the effects of the E term (proportional to φ^2) have been made and the critical exponent ν describing the divergence of the correlation length ξ near T_a has been determined. This investigation will be reported separately as it is not the subject of the present paper but it employs the results obtained here.[23]

ACKNOWLEDGMENTS

The authors would like to thank E. O. Schulz-Du Bois for his contribution to the calculation of second-order terms in the theoretical part and a critical reading of the manuscript, as well as F. Waldner for discussions.

[1] E. S. Kirkpatrick, K. A. Müller, and R. S. Rubins, Phys. Rev. 135, A86 (1964).
[2] R. Baer, G. Wessel, and R. S. Rubins, J. Appl. Phys. 39, 23 (1968).
[3] R. G. Pontin, E. F. Slade, and D. J. E. Ingram, J. Phys. C 2, 1146 (1969).
[4] D. J. A. Gainon, J. Appl. Phys. 36, 2325 (1965).
[5] D. M. Hannon, Phys. Rev. 164, 366 (1967).
[6] K. A. Müller, W. Berlinger, and R. S. Rubins, Phys. Rev. 186, 361 (1969).
[7] B. W. Faughnan, RCA Internal Report, 1969 (unpublished).
[8] D. M. Hannon, Phys. Status Solidi 43, K21 (1971).
[9] D. M. Hannon, Phys. Rev. (to be published).
[10] K. A. Müller, W. Berlinger, and F. Waldner, Phys. Rev. Letters 21, 814 (1968).

[11]H. Unoki and T. Sakudo, J. Phys. Soc. Japan 23, 546 (1967).
[12]J. C. Slonczewski and H. Thomas, Phys. Rev. B 1, 3599 (1970).
[13]K. A. Müller and W. Berlinger, Phys. Rev. Letters 26, 13 (1971).
[14]K. A. Müller, W. Berlinger, and J. C. Slonczewski, Phys. Rev. Letters 25, 734 (1970).
[15]K. A. Müller, Helv. Phys. Acta 31, 173 (1958).
[16]K. A. Müller, W. Berlinger, M. Capizzi, and H. Gränicher, Solid State Commun. 8, 549 (1970).
[17]B. Alefeld, Z. Physik 222, 155 (1969).
[18]D. A. Jones, J. M. Baker, and D. F. D. Pope, Proc. Phys. Soc. (London) 74, 249 (1959).
[19]B. Henderson, J. E. Wertz, T. P. P. Hall, and R. D. Dowsing, J. Phys. C 4, 107 (1971).
[20]See, for instance, E. U. Condon and G. H. Shortley, *The Theory of Atomic Spectra* (Cambridge U. P., Cambridge, 1957), p. 34.
[21]K. A. Müller, in *Structural Phase Transitions and Soft Modes*, edited by E. J. Samuelsen, E. Andersen, and J. Feder (Universitetsforlaget, Oslo, Norway, 1971), p. 85.
[22]F. Schwabl, Phys. Rev. Letters 28, 500 (1972).
[23]Th. von Waldkirch, K. A. Müller, W. Berlinger, and H. Thomas, Phys. Rev. Letters 28, 503 (1972).

PHYSICAL REVIEW B VOLUME 5, NUMBER 11 1 JUNE 1972

Determination of the Sternheimer Antishielding Factor of Li^7 in Lithium Fluoride by Acoustic Nuclear Magnetic Resonance*

J. R. Anderson† and J. S. Karra
Department of Physics, Temple University, Philadelphia, Pennsylvania 19122
(Received 2 August 1971)

An experimental determination of the magnitude of the Sternheimer antishielding factor $1-\gamma_\infty$ for the Li^+ ion by means of acoustic nuclear magnetic resonance (acoustic NMR) of Li^7 in single-crystal LiF is presented. It was found that $|1-\gamma_\infty| = 3.4 \pm 13\%$, corresponding to an antishielding effect. This may be compared with theoretical calculations by other investigators which give $1-\gamma_\infty = 0.75$, a small shielding effect. The shape of the acoustic NMR line for H parallel to the [001] direction was found to be approximately Gaussian with a second moment $\Delta H^2 = (5.1 \pm 0.8)^2\ G^2$. A theoretical calculation of that second moment was carried out, assuming only magnetic dipole-dipole interactions between nuclei, and yielding $\Delta H^2 = 5.9\ G^2$ in good agreement with this experiment. Experimentally, the LiF crystal was cooled in liquid helium to 4.2°K and placed in a steady magnetic field H. Acoustic waves at twice the Li^7 Lamor frequency were introduced into the crystal by means of a piezoelectric transducer. The resulting periodic distortions of the crystal modulated the interaction $\overleftrightarrow{Q}:\nabla\vec{E}$ between the nuclear electric quadrupole moment $\overleftrightarrow{Q}$ and the electric-field gradient $\nabla\vec{E}$ generated transitions among the Zeeman energy levels. These transition rates were measured by observing the rate of change of the amplitude of an ordinary (nonacoustic) NMR signal. The transition rate expected for a point-charge model of the crystal was calculated to be proportional to $(\overleftrightarrow{Q}:\nabla\vec{E})^2$, and, using the known value $Q = 0.043$ barn, was smaller than the experimental transition rate by a factor of 11.8. Additional calculations were made which showed that covalency and overlap should have a negligible effect on ∇E, making it possible to ascribe this factor of 11.8 solely to antishielding. The ratio of the actual transition rate to that calculated is equal to the square of the antishielding factor: $(1-\gamma_\infty)^2 = 11.8$ so that $|1-\gamma_\infty| = 3.4$, with an estimated probable error of 13%.

I. INTRODUCTION

In this paper we report an experimental determination of the Sternheimer antishielding factor for the Li^7 ion in lithium fluoride. The experiment makes use of the method of ultrasonic saturation of the lithium NMR line.

This method was first conceived by Kastler[1] and entails the modulation of the quadrupole coupling energy by means of acoustic waves at the proper frequency to generate transitions among the nuclear Zeeman states. This effect, first demonstrated by Proctor and Tantilla[2] and later by other investigators[3–12] is observed in two different experimental forms. One, the dissipation method, which was developed by Bolef and Menes,[7,8] makes use of the marginal oscillator as in ordinary NMR. The other is the saturation method, used in this present experiment, which depends on the saturation of NMR lines as a consequence of the transitions induced by the acoustic effect.

In the saturation method, one observes the time rate of decrease dS/dt of the NMR signal S. Then if M is the magnetization of the sample,

$$\frac{1}{S}\frac{dS}{dt} = \frac{1}{M}\frac{dM}{dt} = KP\ , \tag{1}$$

where the latter equality depends on the existence